Desalination and Water Treatment
www.deswater.com

doi: 10.1080/19443994.2016.1156028

57 (2016) 25411–25420
November

Taylor & Francis
Taylor & Francis Group

Preparation of spherical mesoporous aminopropyl-functionalized MCM-41 and its application in polyamide thin film nanocomposite reverse osmosis membranes

Guiru Zhu*, Mengru Bao, Zhaofeng Liu, Congjie Gao

Key Laboratory of Marine Chemistry Theory and Technology, Ministry of Education, College of Chemistry and Chemical Engineering, Ocean University of China, Qingdao 266100, China, Tel. +86 0532 66782223; emails: zhugr@ouc.edu.cn (G. Zhu), baomengru@163.com (M. Bao), liuzhaofeng126@126.com (Z. Liu), gaocjie@ouc.edu.cn (C. Gao)

Received 22 September 2015; Accepted 14 February 2016

ABSTRACT

Aminopropyl-functionalized MCM-41 (NH_2-MCM-41) was synthesized by the one-pot hydrothermal method using tetraethoxysilane (TEOS) and (3-aminopropyl)triethoxysilane (APTES) as silica sources, cetyltrimethylammonium bromide as template, ethanol as a cosolvent, and sodium hydroxide as the alkali source. The synthesized nanoparticles were noticeably monodisperse with standard deviation of under 10% for the mean particle size. The specific surface area, pore size, pore volume and amino group density of the NH_2-MCM-41 varied with the content of APTES in the initial solution. The NH_2-MCM-41-polyamide thin film nanocomposite reverse osmosis (TFN RO) membranes were obtained by interfacial polymerization of trimesoyl chloride (TMC) and *m*-phenylene-diamine (MPD). The hydrophilicity of the TFN RO membranes was improved by the incorporation of NH_2-MCM-41 nanoparticles. The water flux of 54 L m^{-2} h^{-1} at 1.6 MPa for NH_2-MCM-41-polyamide TFN RO membrane was nearly 2.8 times that of the pure polyamide thin film composite (TFC) RO membrane and the solute rejection was 96.5% with a 0.1% w/v NH_2-MCM-41 loading.

Keywords: Aminopropyl; MCM-41; Interfacial polymerization; Reverse osmosis; Nonacomposite membranes

1. Introduction

Reverse osmosis (RO) membrane technology has become a dominant method for water purification because of its advantages including a short construction cycle, simple equipment and operation and its low impact on the environment [1]. To reduce the operating costs and energy consumption, RO membranes with higher water permeability, improved rejection and better fouling resistance are needed [2].

Jeong et al. have reported a new concept for the interfacial polymerization of thin film nanocomposite (TFN) RO membrane via embedding zeolite nanoparticles throughout the polyamide thin film layer [3]. The water permeability of these novel RO membranes was dramatically improved by the enhanced hydrophilicity of the membrane, with no significant change in salt rejection. Lind et al. [4] and Fathizadeh et al. [5] used different types of zeolite nanoparticles for the TFN

*Corresponding author.

membranes. In place of zeolite particles, other types of inorganic nanomaterials, such as silica [6], MCM-41 [7], ordered mesoporous carbon [8], aluminosilicate single-walled nanotubes [9], titanium nanotubes [10], halloysite nanotubes [11], and carbon nanotubes [12,13] have been reportedly used as nanofillers embedded in a polyamide layer of TFN RO membranes with the goal of precluding the tradeoff between water permeability and solute selectivity. These studies all showed that the resultant TFN RO membranes exhibited enhanced performance, in particular much higher water flux. The enhancement of water flux was due to the higher hydrophilicity and lower cross-linking density of thin film layer. Additionally, the internal porosity of the nanoparticles/nanotubes can provide flow paths for water molecules through nanocomposite thin film layer. However, the morphology of the nanoparticles is irregular in shape, which is not conducive to their even dispersion in the polyamide layer. In addition, the pore structure of the nanoparticles is oriented which complicates the control of the available flow path for water. The nanotubes with lengths between 10 and 50 μm cannot be accommodated in a thin polyamide layer in a vertical orientation. These issues represent the most significant challenges in this field [14].

In our previous report [15], monodispersed mesoporous nanosilica spheres were incorporated in the polyamide layer of the RO membrane, resulting in a prominent increase in water flux, but a slight decrease in salt rejection. The morphology of the monodispersed mesoporous silica is spherical, making this material easy to disperse. Also, the silica spheres have a radially arranged mesoporous structure emanating from the heart of the particle to the outer surface of the sphere which is randomly oriented.

These inorganic particles were incorporated into a TFN membrane by physical encapsulation. The weak interaction between inorganic particles and polymer matrix is likely to cause easy leaching of the nanomaterials from the membrane which would adversely affect its performance [14]. Wu et al. [16] synthesized amino group functionalized silica nanoparticles using a post-grafting method and prepared a TFN nanofiltration (NF) membrane via interfacial polymerization of trimesoyl chloride (TMC) and piperazine (PIP). The amino groups of the modified silica nanoparticles were found to react with TMC, which produced a covalent bond between the silica particles and the polymer matrix. The resulting TFN membrane exhibited good, long-term stability. Emadzadeh et al. [17] prepared a TFN membrane by dispersing amino functionalized titanate nanotubes (NH_2-TNTs) in an organic phase. Wu et al. [16] and Emadzadeh et al. [17] both employed FTIR spectroscopy to substantiate the presence of chemical bonding between the $-NH_2$ groups on the nanomaterials and the TMC during the process of interfacial polymerization.

Amino functionalized mesoporous silica has attracted much attention as catalysts [18] and adsorbents [19], because of the uniformity of the mesopores, high specific surface area, controllable nanostructure and macroscopic morphologies, as well as the presence of amino groups. Amino-functionalized monodispersed mesoporous silica spheres have been synthesized by modifying the Stöber method [20] with the further addition of a template such as alkyl trimethyl ammonium halide [21] or an anionic surfactant [22]. However, the particle size should match the thin film layer to allow incorporation in the TFN membrane. To date, amino-functionalized monodispersed mesoporous silica spheres used as nanoparticles in TFN RO membranes have not been reported.

In the present study, monodispersed mesoporous aminopropyl-functionalized MCM-41 nanospheres were synthesized using the one-pot co-condensation hydrothermal method and characterized by FTIR, BET, X-ray diffraction (XRD), SEM and TEM. Then, monodispersed spherical mesoporous NH_2-MCM-41-polyamide TFN RO membranes were prepared by incorporating the nanoparticles into a thin film polyamide membrane via interfacial polymerization of trimesoyl chloride (TMC) and *m*-phenylene-diamine (MPD). The influence of the quantity of nanoparticles in the membrane on the membrane performance was investigated in terms of water flux and salt rejection.

2. Experimental

2.1. Materials

Cetyltrimethylammonium bromide (C_{16}TAB) was obtained from Guangfu Chemical Group (Tianjin, China). Tetraethoxysilane (TEOS) was obtained from Sinopharm Chemical Reagent (Shanghai, China). (3-aminopropyl)triethoxysilane (APTES) was obtained from Chenguang Silane Co., Ltd (Jiangsu, China). Polysulfone (P-3500 PS) and *m*-phenylenediamine (MPD) were purchased from Solvay (USA). Trimesoyl chloride (TMC) was obtained from Sigma-Aldrich (USA). All chemicals were analytical grade and used without further purification. Deionized water used in all experiments was produced by Milli-Q water purification system.

2.2. Preparation of mesoporous aminopropyl-functionalized MCM-41 nanospheres

Mesoporous aminopropyl-functionalized MCM-41 nanospheres were synthesized from the TEOS-APTES-C_{16}TAB-EtOH-NaOH system using the hydrothermal method. In a typical procedure, the surfactant C_{16}TAB (0.205 g) was dissolved in deionized water (90 mL) containing 2 M NaOH (0.7 mL) and ethanol (10 mL), with stirring at 80˚C to obtain a clear solution. Then, the mixture of TEOS (1.111 g) and APTES (0.132 g) was added to the clear solution with vigorous stirring. After 2 h of continuous stirring at 80˚C, a white precipitate was collected by filtration, washed with ethanol at least three times, and dried at 60˚C for 12 h. The molar ratio was C_{16}TAB:H_2O:EtOH:NaOH:APTES:TEOS = 0.106:930.4:31.87:0.271:y:1 with y = 0–0.332. The surfactant was extracted by stirring 1.0 g of the synthesized sample in 150 mL of ethanol containing 5 mL 36 wt% HCl aqueous solution for 6 h at 70˚C. After filtration, the sample was washed thoroughly with ethanol and dried in air at 60˚C overnight. The sample was denoted as x-NH_2-MCM-41, where x refers to the molar percentage of APTES/(TEOS + APTES).

2.3. Characterization of x-NH_2-MCM-41 nanospheres

FT-IR spectra were recorded on a Thermo Nicolet Impact 750 FT-IR spectrometer using a KBr pellet. Powder XRD patterns were recorded on a Rigaku D/MAX 2500 powder diffraction system using Cu Kα radiation. SEM images were obtained using an S-4800 (Hitachi) system. The sample was deposited on a sample holder with an adhesive carbon foil and sputtered with gold before measurement. TEM images were obtained using a JEM-2100 system at an acceleration voltage of 200 kV. Nitrogen sorption experiments were performed at 77 K using an ASAP 2020 analyzer. The sample was pretreated at 373 K before the measurement. The Brunauer–Emmett–Teller (BET) surface areas were calculated from the adsorption data. The pore size distribution curve was obtained from the adsorption branched using the Barrett–Joyner–Halenda (BJH) method. Elemental analysis was performed using an Elementar Vario PE2400 apparatus.

2.4. Preparation of the NH_2-MCM-41-polyamide TFN RO membranes

The polysulfone (PSF) porous support membrane preparation was conducted as follows [15]. The casting solution was prepared from 73.6% DMF + 8.0% PEG-400 + 0.4% H_2O + 18% polysulfone at 60˚C for 24 h with stirring. After leaving this solution undisturbed for 24 h, it was spread on a glass plate with a glass knife and immersed into a gelation bath after evaporating the solvent for 30 s at room temperature. The polysulfone porous support membrane was then obtained and stored in deionized water.

The NH_2-MCM-41-polyamide TFN RO membranes were prepared via interfacial polymerization. A polysulfone support was fixed between two square wooden frames using four clips, and an appropriate amount of 2.0% (w/v) MPD aqueous solution containing 0.0–0.1% (w/v) mesoporous NH_2-MCM-41 nanoparticles was poured onto the PSF membrane. The NH_2-MCM-41 nanoparticle dispersion was prepared by ultrasonication for 30 min at room temperature before interfacial polymerization. The MPD solution was rolled back and forth with a rubber roller for 3 min on the membrane to ensure that the membrane was saturated by MPD. After the excess aqueous solution was removed, the PSF support was dried vertically in air for 2 min. Subsequently, 0.1% (w/v) TMC solution in hexane was poured onto the PSF membrane for 55 s for interfacial polymerization and air dried for 5 s. The resulting membrane was placed in a hot air circulating oven maintained at 115˚C for 3 min to achieve stabilization.

2.5. Membrane characterizations

Images of the surface and cross-section of the NH_2-MCM-41-polyamide TFN RO membranes were obtained using a S-4800 (Hitachi) system. Energy dispersive X-ray (EDX) spectroscopy (equipped with SEM) was used to determine the elemental compositions of the synthesized membranes. The contact angles of deionized water of the synthesized NH_2-MCM-41-polyamide TFN RO membranes were measured using a contact angle goniometer (DSA100, KRÜSS) by the sessile drop method.

The membranes were evaluated in a flow cell of the RO test kit at room temperature with an effective membrane area of 19.625 cm^2 and operating pressure of 1.6 MPa. The performance of the membranes was determined using 2,000 ppm NaCl solution. After the membranes were compressed for 30 min at 1.6 MPa, the water flux was measured. Three coupons from each membrane were evaluated to determine average water flux and solute rejections The water flux (F) and salt rejection (R) were calculated in Eqs. (1) and (2), respectively:

$$F = \frac{Q}{A \cdot \Delta t} \quad (1)$$

$$R = \left(1 - \frac{K_p}{K_f}\right) \times 100\% \quad (2)$$

where Q (L) is the volume of water collected within the time period Δt (h), A (m^2) is the effective membrane area, and K_p and K_f ($\mu S\ cm^{-1}$) are the conductivity of the permeate and feed solutions, respectively.

3. Results and discussion

3.1. Characterizations of NH_2-MCM-41

3.1.1. FT-IR

Fig. 1 shows the FT-IR spectra of as-synthesized 10-NH_2-MCM-41, extracted MCM-41 and x-NH_2-MCM-41 with different molar percentage of APTES (x = 5–25) in the initial solution. Compared with as-synthesized 10-NH_2-MCM-41 (as-10-NH_2-MCM-41), the intensity of the bands assigned to C_{16}TAB (2,922 and 2,854 cm^{-1} [23]) are significantly decreased in the FT-IR spectrum of the extracted x-NH_2-MCM-41, indicating that most of the surfactant had been removed by the solvent extraction method (Fig. 1(a)). Compared to MCM-41, several new infrared absorption bands can be observed in the samples of x-NH_2-MCM-41 (Fig. 1(b)). The band at 1,510 cm^{-1} corresponds to the symmetric N–H bending vibration of $-NH_3^+$ [24,25], indicating that the free amine groups were protonated to form protonated amine species during the extraction of the surfactant in an acid medium. The bands at 1,470 and 1,449 cm^{-1} can be attributed to the bending vibrations of C–H in the propyl group of APTES [26]. The band at 1,414 cm^{-1} is related to the C–H vibrations of bridging $-CH_2CH_2-$ groups [27]. The results confirmed the existence of aminopropyl groups in the x-NH_2-MCM-41. The band at 795 cm^{-1} corresponds to the symmetric Si–O stretching vibration. The intensity ratio of the band at 1,510 cm^{-1} (N–H) and at 795 cm^{-1} (Si–O) increased with the increase of the amount of APTES in the initial solution. This indicated that the density of $-NH_2$ group on the synthesized materials increased with the increment of APTES in the initial solution.

3.1.2. SEM

Fig. 2 shows the SEM images of MCM-41 and x-NH_2-MCM-41 prepared with different APTES molar ratios. It can be seen that all the samples exhibited a spherical shape. The SEMs revealed that the all samples exhibited a standard deviation of under 10% in the mean particle size, which indicated that they were noticeably monodisperse. This indicated that the addition of APTES did not influence the monodispersity of the particles. But the particle size gradually increased with the increase in the APTES molar percentage (Table 1). Under basic conditions, the neutral $-NH_2$ of APTES can interact with each other through hydrogen bonding, which can slow the condensation of hydrolyzed-$Si(OH)_n(OR)_{3-n}$ species around the C_{16}TAB micelles. At higher APTES contents, the steric hindrance between hydrolyzed-APTES species was greatly enhanced. As a result, the rate of condensation of the hydrolyzed-$Si(OH)_n(OR)_{3-n}$ and APTES around the surfactant micelles was retarded. The slow condensation rate of the silane species was helpful in the formation of spheres with larger diameters. The total

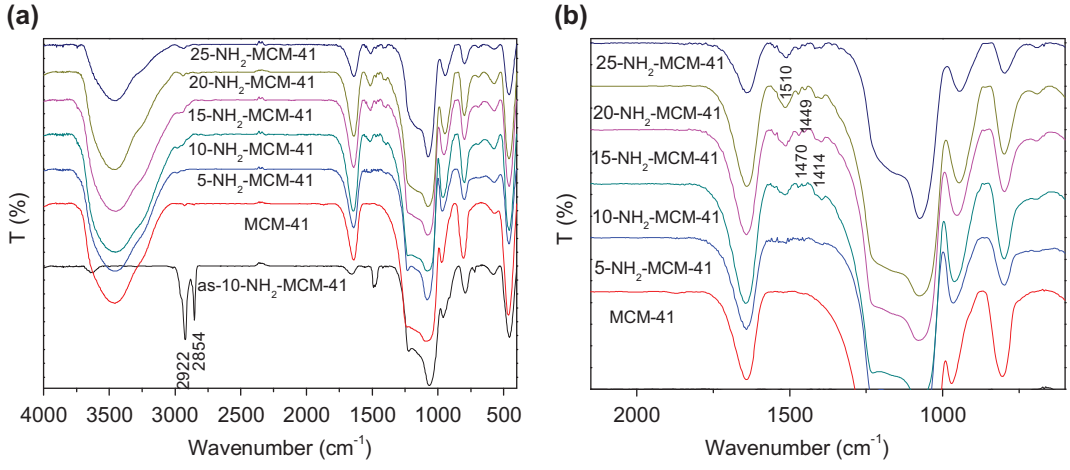

Fig. 1. FT-IR spectra of as-synthesized 10-NH_2-MCM-41, extracted MCM-41 and x-NH_2-MCM-41 particles (a) and detail view on the characteristic band of aminopropyl groups is presented (b).

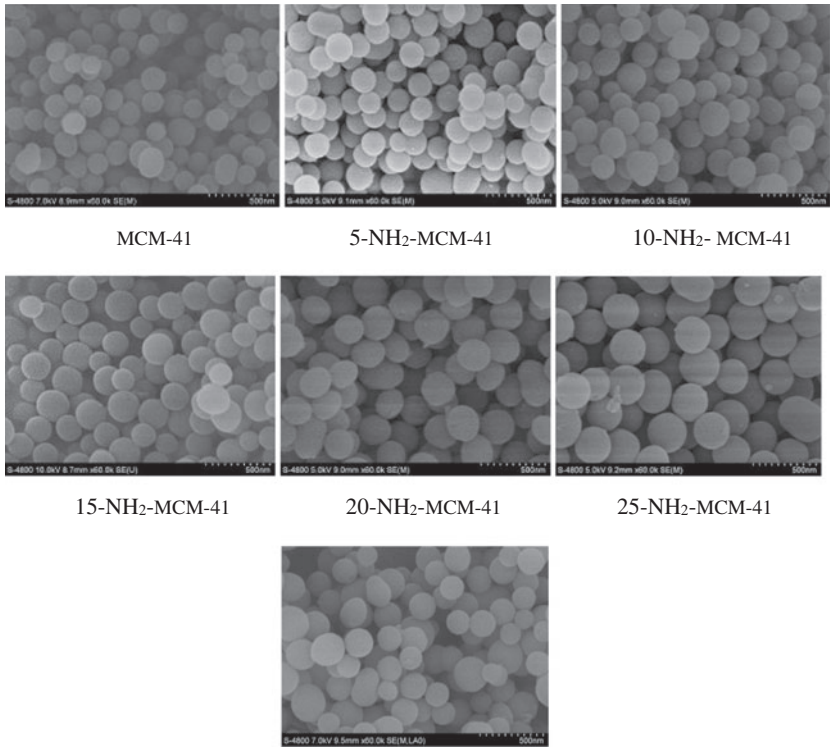

Fig. 2. SEM characterizations of MCM-41 and x-NH_2-MCM-41 with different APTES molar ratios (x = 5–25), and MCM-41-200 is the MCM-41 with average particle size of 200 nm.

Table 1
Textural features of MCM-41 and x-NH_2-MCM-41 particles with different APTES molar ratios (x = 5–25)

Sample	APTES	S_{BET} ($m^2\ g^{-1}$)	Pore volume ($cm^3\ g^{-1}$)	Pore size (nm)	Particle diameter (nm)	NH_2 density (mmol g^{-1})	RSD (%)
MCM-41	0	1,141	0.77	2.68	164	–	4.87
5-NH_2-MCM-41	5%	1,044	0.76	2.71	183	0.009	6.34
10-NH_2-MCM-41	10%	1,007	0.73	2.74	192	0.503	5.76
15-NH_2-MCM-41	15%	1,010	0.71	2.51	209	1.044	6.49
20-NH_2-MCM-41	20%	957	0.70	2.53	235	1.382	9.14
25-NH_2-MCM-41	25%	731	0.42	2.53	284	1.536	3.21
MCM-41-200	0	1,057	0.74	2.79	200	–	5.19

concentration of the silane increased with the increase in the amount of the APTES, resulting in larger particle sizes. Therefore, the spheres with a large particle size can be formed with higher APTES content.

3.1.3. XRD

The mesoporous structures of MCM-41 and x-NH_2-MCM-41 particles were investigated using powder XRD. The XRD patterns of the samples are shown in Fig. 3. MCM-41 displayed three resolved diffraction peaks corresponding to (1 0 0), (1 1 0) and (2 0 0) reflections, characteristic of the mesoporous material with an ordered two-dimensional (2D)-hexagonal mesostructure [28]. Compared with MCM-41, the (1 0 0) diffraction peak intensity of x-NH_2-MCM-41 was evidently decreased, and the (1 1 0) and (2 0 0) reflections overlapped to become a broad, weak peak and disappeared as x was increased from 5 to 15. There was no diffraction peak in the XRD patterns of the 20-NH_2-MCM-41 and 25-NH_2-MCM-41 (not shown here). The XRD results indicated that APTES

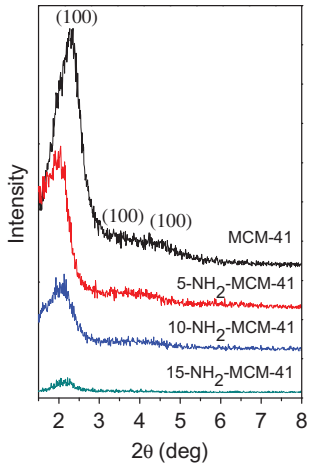

Fig. 3. XRD patterns of MCM-41 and x-NH_2-MCM-41 particles with different APTES molar ratios (x = 5–15).

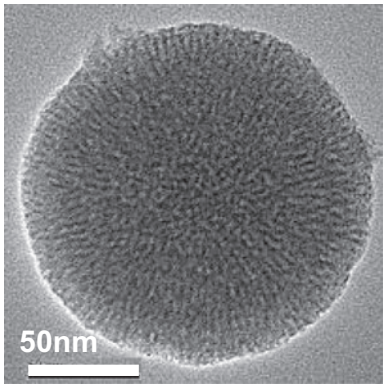

Fig. 4. TEM image of 10-NH_2-MCM-41.

disturbed the ordered assembly of the silicate species around the surfactant micelles, especially at high APTES concentration. This was due to the APTES, which only has three $-OC_2H_5$ groups. Therefore, lattice defects were formed via co-condensation of APTES with TEOS. There were more lattice defects with higher contents of APTES in the initial solution. As a result, the weak ordered or disordered mesostructure of 10-NH_2-MCM-41 were obtained. The TEM image of 10-NH_2-MCM-41 in Fig. 4 shows that the spherical NH_2-functionalized MCM-41 nano-particles are mesoporous materials and have a pore structure radiating from the heart of the particle to the outer surface of the sphere.

3.1.4. BET

N_2 adsorption–desorption isotherms and the corresponding BJH pore size distribution curves of the extracted samples are shown in Fig. 5. The adsorption–desorption isotherms for all samples are type IV isotherms with a sharp capillary condensation step, which is characteristic of mesoporous materials with narrow pore size distributions. The BET specific surface area, the pore volume and the pore diameter of the materials are summarized in Table 1. Compared with the MCM-41, a decrease of surface area, pore volume and pore diameter can be seen in the x-NH_2-MCM-41 and the data showed a further decrease with higher APTES concentration. The elemental analysis of x-NH_2-MCM-41 demonstrated that NH_2 density in the samples increased as the concentration of APTES in the initial solution increased (Table 1). Therefore, the decrease in surface area, pore volume and pore diameter of the sample synthesized with a higher APTES molar ratio may result from the fact that higher amounts of APTES incorporated in the mesopore may fill the porous spaces in the mesoporous materials.

In regard to the morphology, particle size and mesostructural order, the 10-NH_2-MCM-41 with a spherical morphology, 192 nm particle size and ordered mesoporous structure is a desirable material for use as nanoparticles to prepare TFN RO membranes. For comparison, MCM-41 particles with a diameter of 200 nm (MCM-41-200) were used to prepare the MCM-41-polyamide TFN RO membrane. The preparation process of MCM-41-200 is similar with NH_2-MCM-41 with the molar ratio of C_{16}TAB:H_2O:EtOH:NaOH:TEOS = 0.106:930.4:31.87:0.347:1. The SEM image of MCM-41-200 is shown in Fig. 2 and the textural features are listed in Table 1.

3.2. Characterizations of the NH_2-MCM-41-polyamide TFN RO membranes

3.2.1. Surface morphology

The SEM images of the surface of the pure polyamide TFC membrane and NH_2-MCM-41-polyamide TFN RO membranes are shown in Fig. 6. Spherical particles are visible on all NH_2-MCM-41-polyamide TFN RO membranes surface in Fig. 6(b)–(f). As can be seen, the amount of nanoparticles per membrane unit area gradually increased from (b) to (f) with the increase of NH_2-MCM-41 loading. At low NH_2-MCM-41 loadings, Fig. 6(b)–(d), the nanoparticles are uniformly distributed in the synthesized membranes. This dominant result benefited from the spherical morphology of the synthesized mesoporous NH_2-MCM-41. However, at higher NH_2-MCM-41 loadings (Fig. 6(e) and (f)), the nanoparticles aggregated. This result indicated that the amount of NH_2-MCM-41 embedded in the membrane should be tightly controlled to achieve

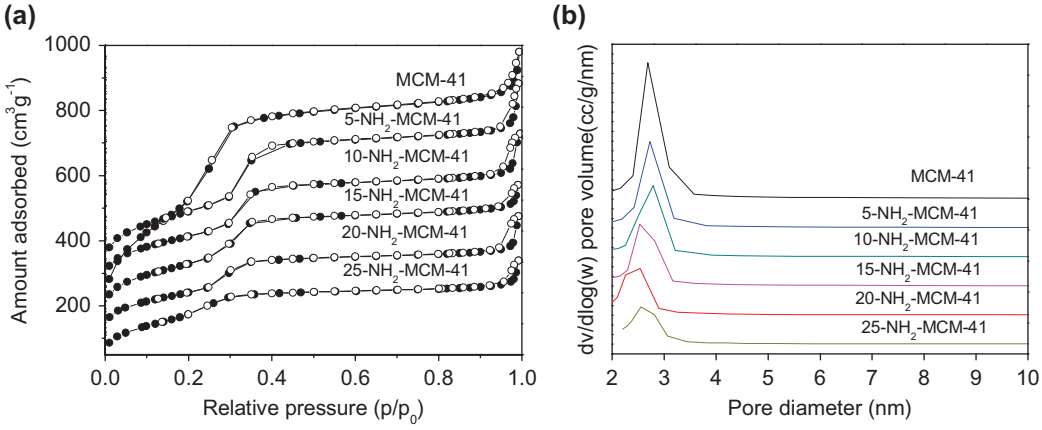

Fig. 5. N_2 adsorption–desorption isotherms (a) and pore size distribution curves (b) of MCM-41 and *x*-NH_2-MCM-41 particles with different APTES molar ratios (*x* = 5–15).

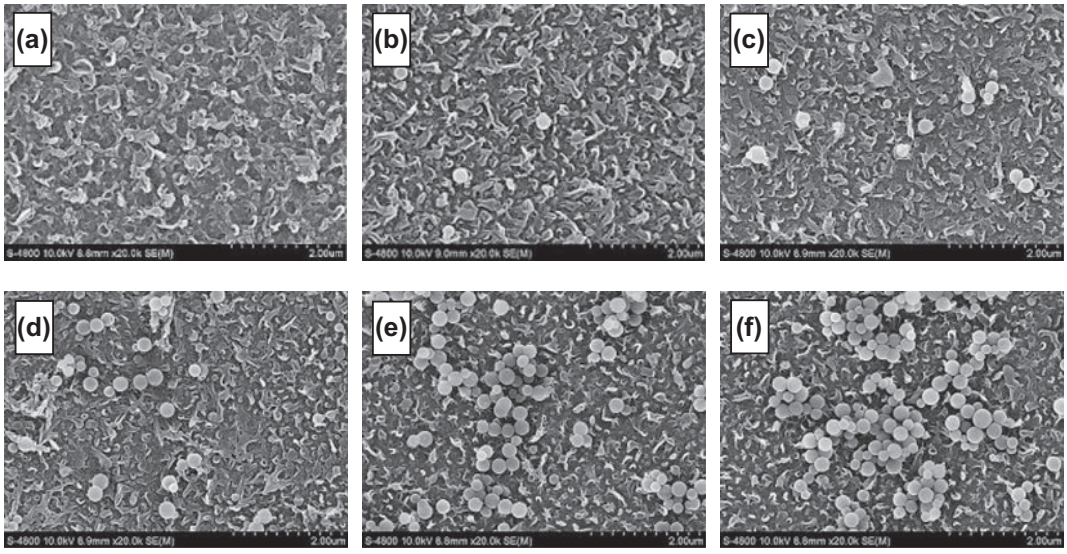

Fig. 6. SEM images of (a) pure polyamide TFC RO membrane and (b–f) NH_2-MCM-41-polyamide TFN RO membranes. The amount (w/v%) of mesoporous 10-NH_2-MCM-41 nanoparticles contained in the MPD aqueous was (b) 0.005%, (c) 0.01%, (d) 0.04%, (e) 0.08% and (f) 0.1%.

uniform nanoparticle distribution. As shown in Fig. 6, it can be seen that, as the content of the NH_2-MCM-41 was increased, the surface morphological structure of the membranes changed from "leaf-like" in the pure polyamide TFC RO membrane to "ridge and valley" in the NH_2-MCM-41-polyamide TFN RO membranes. This means that the NH_2-MCM-41-polyamide TFN RO membranes became smoother as the NH_2-MCM-41 contents increased. That may be caused by hydrogen bonding between polyamide layer and NH_2-MCM-41 nanoparticles. This decline in surface roughness of the membrane with the embedment of hydrophilic nanoparticles has also been observed in other studies [5].

3.2.2. Cross-sectional structures

The SEM images and EDX spectra of the cross-sections of pure polyamide TFC RO membrane and mesoporous NH_2-MCM-41-polyamide TFN RO membrane with dispersing 0.08 w/v% 10-NH_2-MCM-41 in aqueous phase are illustrated in Fig. 7. Spherical particles are visible in the polyamide skin layer of the mesoporous NH_2-MCM-41-polyamide TFN RO membrane (Fig. 7(e)). The EDX spectrum in Fig. 7(f) shows a Si peak at ~1.7 keV, confirming the presence of NH_2-MCM-41, which is absent in the pure polyamide TFC RO membranes in Fig. 7(b) and the corresponding EDX spectrum shown in Fig. 7(c).

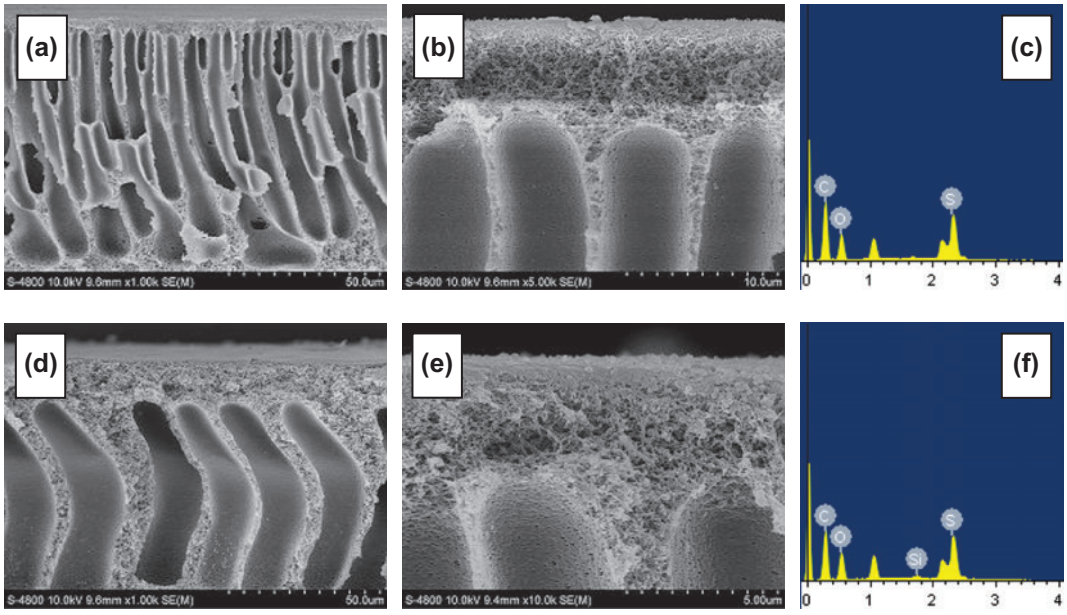

Fig. 7. SEM and EDX characterizations of the cross-sectional structures of (a–c) pure polyamide TFC RO membrane and (d–f) mesoporous NH_2-MCM-41-polyamide TFN RO membrane.

For comparison, mesoporous pure silica (MCM-41-200) with a similar particle size, pore size, surface area and pore volume with that of 10-NH_2-MCM-41 was used as nanoparticles for the synthesis of a MCM-41-polyamide TFN RO membrane.

The influence of the mesoporous 10-NH_2-MCM-41 loading on the surface properties of NH_2-MCM-41-polyamide TFN RO membrane and the MCM-41-200 loading on the surface properties of MCM-41-polyamide TFN RO membrane are demonstrated in Fig. 8. The water contact angle of the membranes gradually decreased with the increase in nanoparticle loading. Hence, the hydrophilicity of the membranes increased with the increase in nanoparticle loading. This result was similar to with our previous results [15]. The water contact angle of the NH_2-MCM-41-polyamide TFN RO membrane was less than that of the MCM-41-polyamide TFN RO membrane synthesized with same amount of added nanoparticles. This indicated that the NH_2-MCM-41-polyamide TFN RO membrane was more hydrophilic. The hydrophilicity of the NH_2-MCM-41-polyamide TFN RO membranes was improved by the numerous hydrophilic hydroxyl groups and amino groups in the internal surfaces of the mesoporous NH_2-MCM-41. Due to the structure of the APTES, the amino groups were connected to the Si by $–CH_2–CH_2–CH_2–$ groups, and the –OH groups were connected to the –O– groups. Therefore, the amino groups is further from the surface of the nanoparticle than hydroxyl groups and can easily interact with H_2O, resulting higher hydrophilicity of the NH_2-MCM-41-polyamide TFN RO membrane.

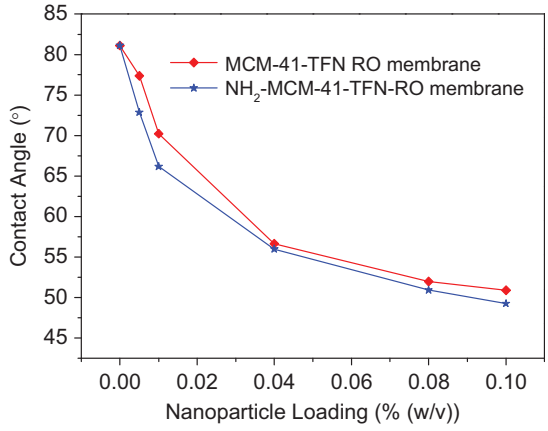

Fig. 8. Effect of mesoporous 10-NH_2-MCM-41 and MCM-41-200 loading on surface properties of synthesized NH_2-MCM-41-polyamide TFN RO membrane (★) and MCM-41-polyamide TFN RO membrane (♦), respectively.

3.2.3. RO performance

The separation properties of the synthesized TFN RO membranes are shown in Fig. 9. The water flux of NH_2-MCM-41-polyamide TFN RO membrane and MCM-41-polyamide TFN RO membrane increases with the increase in the quantity of nanoparticles.

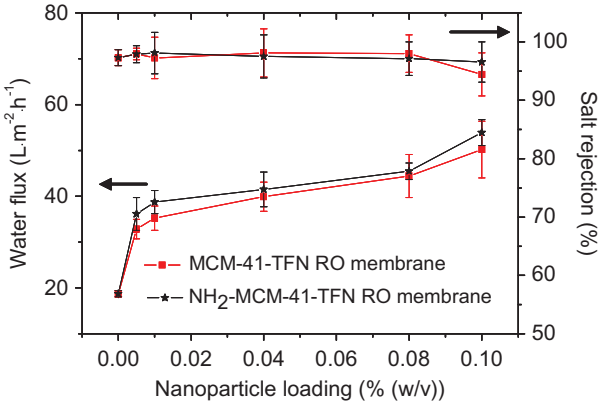

Fig. 9. Effect of mesoporous 10-NH_2-MCM-41 and MCM-41-200 loading on separation performance of synthesized NH_2-MCM-41-polyamide TFN RO membrane (★) and MCM-41-polyamide TFN RO membrane (■), respectively.

Also, the water flux of NH_2-MCM-41-polyamide TFN RO membrane was higher than the MCM-41-polyamide TFN RO membrane synthesized with same quantity of nanoparticles. The enhanced permeability of the synthesized membranes was due to the higher hydrophilicity of NH_2-MCM-41-polyamide TFN RO membranes containing mesoporous NH_2-MCM-41 with numerous hydrophilic hydroxyl and amino groups, which was confirmed by the contact angle analysis. The solute rejection of all the synthesized membranes was greater than 96%. By adding 0.1% w/v mesoporous 10-NH_2-MCM-41 into the aqueous phase, the water flux (54 L m^{-2} h^{-1}) of the NH_2-MCM-41-polyamide TFN RO membrane was nearly 2.8 times greater than that of the pure polyamide TFC RO membrane. This indicated that the NH_2-MCM-41 nanoparticle is a promising nanofiller for improving the properties if the TFN RO membrane provides it with high water flux and salt rejection.

4. Conclusions

Monodispersed spherical aminopropyl-functionalized MCM-41 was synthesized by the one-pot hydrothermal method. Several NH_2-MCM-41-polyamide TFN RO membranes were prepared using interfacial polymerization. When the concentration of NH_2-MCM-41 was 0.1 wt% in the aqueous phase, the water flux (54 L m^{-2} h^{-1}) of the TFN RO membrane was 2.8 times better than the pure polyamide TFC RO membrane at 1.6 MPa operating pressure, while the salt rejection (96.5%) remained comparable with that of pure polyamide TFC RO membrane. These results indicated that the monodispersed spherical mesoporous NH_2-MCM-41, due to its super hydrophilicity, spherical morphology and amino groups, may be particularly useful in improving the water flux of TFN RO membranes.

Acknowledgement

This work is financially supported by the National Natural Science Foundation of China (No. 21276246).

References

[1] A.P. Rao, N.V. Desai, R. Rangarajan, Interfacially synthesized thin film composite RO membranes for seawater desalination, J. Membr. Sci. 124 (1997) 263–272.
[2] C. Kong, A. Koushima, T. Kamada, T. Shintani, M. Kanezashi, T. Yoshioka, T. Tsuru, Enhanced performance of inorganic-polyamide nanocomposite membranes prepared by metal-alkoxide-assisted interfacial polymerization, J. Membr. Sci. 366 (2011) 382–388.
[3] B.H. Jeong, E.M.V. Hoek, Y. Yan, A. Subramani, X. Huang, G. Hurwitz, A.K. Ghosh, A. Jawor, Interfacial polymerization of thin film nanocomposites: A new concept for reverse osmosis membranes, J. Membr. Sci. 294 (2007) 1–7.
[4] M.L. Lind, A.K. Ghosh, A. Jawor, X. Huang, W. Hou, Y. Yang, E.M.V. Hoek, Influence of zeolite crystal size on zeolite-polyamide thin film nanocomposite membranes, Langmuir 25 (2009) 10139–10145.
[5] M. Fathizadeh, A. Aroujalian, A. Raisi, Effect of added NaX nano-zeolite into polyamide as a top thin layer of membrane on water flux and salt rejection in a reverse osmosis process, J. Membr. Sci. 375 (2011) 88–95.
[6] G.L. Jadav, P.S. Singh, Synthesis of novel silica-polyamide nanocomposite membrane with enhanced properties, J. Membr. Sci. 328 (2009) 257–267.
[7] J. Yin, E. Kim, J. Yang, B.L. Deng, Fabrication of a novel thin-film nanocomposite (TFN) membrane containing MCM-41 silica nanoparticles (NPs) for water purification, J. Membr. Sci. 423–424 (2012) 238–246.
[8] E. Kim, B.L. Deng, Fabrication of polyamide thin-film nano-composite (PA-TFN) membrane with hydrophilized ordered mesoporous carbon (H-OMC) for water purifications, J. Membr. Sci. 375 (2011) 46–54.
[9] G.N.B. Baroña, J. Lim, M. Choi, B. Jung, Interfacial polymerization of polyamide-aluminosilicate SWNT nanocomposite membranes for reverse osmosis, Desalination 325 (2013) 138–147.
[10] D. Emadzadeh, W.J. Lau, M. Rahbari-Sisakht, A. Daneshfar, M. Ghanbari, A. Mayahi, T. Matsuura, A.F. Ismail, A novel thin film nanocomposite reverse osmosis membrane with superior anti-organic fouling affinity for water desalination, Desalination 368 (2015) 106–113.
[11] M. Ghanbari, D. Emadzadeh, W.J. Lau, T. Matsuura, A.F. Ismail, Synthesis and characterization of novel thin film nanocomposite reverse osmosis membranes with improved organic fouling properties for water desalination, RSC Adv. 5 (2015) 21268–21276.

[12] L. Zhang, G.Z. Shi, S. Qiu, L.H. Cheng, H.L. Chen, Preparation of high-flux thin film nanocomposite reverse osmosis membranes by incorporating functionalized multi-walled carbon nanotubes, Desalin. Water Treat. 34 (2011) 19–24.
[13] H.Y. Zhao, S. Qiu, L.G. Wu, L. Zhang, H.L. Chen, C.J. Gao, Improving the performance of polyamide reverse osmosis membrane by incorporation of modified multi-walled carbon nanotubes, J. Membr. Sci. 450 (2014) 249–256.
[14] W.J. Lau, S. Gray, T. Matsuura, D. Emadzadeh, J.P. Chen, A.F. Ismail, A review on polyamide thin film nanocomposite (TFN) membranes: History, applications, challenges and approaches, Water Res. 80 (2015) 306–324.
[15] M.R. Bao, G.R. Zhu, L. Wang, M. Wang, C.J. Gao, Preparation of monodispersed spherical mesoporous nanosilica-polyamide thin film composite reverse osmosis membranes via interfacial polymerization, Desalination 309 (2013) 261–266.
[16] H.Q. Wu, B.B. Tang, P.Y. Wu, Optimizing polyamide thin film composite membrane covalently bonded with modified mesoporous silica nanoparticles, J. Membr. Sci. 428 (2013) 341–348.
[17] D. Emadzadeh, W.J. Lau, M. Rahbari-Sisakht, H. Ilbeygi, D. Rana, T. Matsuura, A.F. Ismail, Synthesis, modification and optimization of titanate nanotubes-polyamide thin film nanocomposite (TFN) membrane for forward osmosis (FO) application, Chem. Eng. J. 281 (2015) 243–251.
[18] T.M. Suzuki, M. Yamamoto, K. Fukumoto, Y. Akimoto, K. Yano, Investigation of pore-size effects on base catalysis using amino-functionalized monodispersed mesoporous silica spheres as a model catalyst, J. Catal. 251 (2007) 249–257.
[19] K. Xia, R.Z. Ferguson, M. Losier, N. Tchoukanova, R. Brüning, Y. Djaoued, Synthesis of hybrid silica materials with tunable pore structures and morphology and their application for heavy metal removal from drinking water, J. Hazard. Mater. 183 (2010) 554–564.
[20] W. Stöber, A. Fink, E. Bohn, Controlled growth of monodisperse silica spheres in the micron size range, J. Colloid Interface Sci. 26 (1968) 62–69.
[21] T.M. Suzuki, T. Nakamura, K. Fukumoto, M. Yamamoto, Y. Akimoto, K. Yano, Direct synthesis of amino-functionalized monodispersed mesoporous silica spheres and their catalytic activity for nitroaldol condensation, J. Mol. Catal. A: Chem. 280 (2008) 224–232.
[22] L. Han, Q.R. Chen, Y. Wang, C.B. Gao, S.A. Che, Synthesis of amino group functionalized monodispersed mesoporous silica nanospheres using anionic surfactant, Microporous Mesoporous Mater. 139 (2011) 94–103.
[23] G.R. Zhu, Q.H. Yang, D.M. Jiang, J. Yang, L. Zhang, Y. Li, C. Li, Synthesis of bifunctionalized mesoporous organosilica spheres for high-performance liquid chromatography, J. Chromatogr. A 1103 (2006) 257–264.
[24] A.S.M. Chong, X.S. Zhao, Functionalization of SBA-15 with APTES and characterization of functionalized materials, J. Phys. Chem. B 107 (2003) 12650–12657.
[25] X.G. Wang, K.S.K. Lin, J.C.C. Chan, S. Cheng, Direct synthesis and catalytic applications of ordered large pore aminopropyl-functionalized SBA-15 mesoporous materials, J. Phys. Chem. B 109 (2005) 1763–1769.
[26] L. Zhang, J. Liu, J. Yang, Q.H. Yang, C. Li, Direct synthesis of highly ordered amine-functionalized mesoporous ethane-silicas, Microporous Mesoporous Mater. 109 (2008) 172–183.
[27] L. Zhang, Q. Yang, W.H. Zhang, Y. Li, J. Yang, D. Jiang, G. Zhu, C. Li, Highly ordered periodic mesoporous ethanesilica synthesized under neutral conditions, J. Mater. Chem. 15 (2005) 2562–2568.
[28] J.S. Beck, J.C. Vartuli, W.J. Roth, M.E. Leonowicz, C.T. Kresge, K.D. Schmitt, C.T.W. Chu, D.H. Olson, E.W. Sheppard, S.B. McCullen, J.B. Higgins, J.L. Schlenker, A new family of mesoporous molecular sieves prepared with liquid-crystal templates, J. Am. Chem. Soc. 114 (1992) 10834–10843.